Phonon-induced optical dephasing in single organic molecules

Chloe Clear,[1] Ross C. Schofield,[2] Kyle D. Major,[2] Jake Iles-Smith,[3] Alex S. Clark,[2] and Dara P. S. McCutcheon[1]

[1] *Quantum Engineering Technology Labs, H. H. Wills Physics Laboratory and Department of Electrical and Electronic Engineering, University of Bristol, BS8 1FD, United Kingdom*

[2] *Centre for Cold Matter, Blackett Laboratory, Imperial College London, Prince Consort Road, SW7 2AZ London, United Kingdom*

[3] *Department of Physics and Astronomy, University of Sheffield, Sheffield, S3 7RH, United Kingdom*

(Dated: March 19, 2020)

We present a joint experiment–theory analysis of the temperature-dependent emission spectra, zero-phonon linewidth, and second-order correlation function of light emitted from a single organic molecule. We observe spectra with a zero-phonon-line together with several additional sharp peaks, broad phonon sidebands, and a strongly temperature dependent homogeneous broadening. Our model includes both localised vibrational modes of the molecule and a thermal phonon bath, which we include non-perturbatively, and is able to capture all observed features. For resonant driving we measure Rabi oscillations that become increasingly damped with temperature, which our model naturally reproduces. Our results constitute an essential characterisation of the photon coherence of molecules, paving the way to their use in future quantum information applications.

Deterministic sources of indistinguishable single photons are a key requirement for many quantum information applications [1, 2]. In recent years single molecules of dibenzoterrylene (DBT) have emerged as a promising platform to develop such a source due to a range of desirable properties such as high photostability, high quantum yield [3], favourable absorption and emission wavelengths [4], a high branching ratio to the zero-phonon line (ZPL) [5] and wavelength tunability across their entire inhomogeneous distribution [6]. DBT can exhibit a lifetime-limited ZPL at cryogenic temperatures ($\leq$ 4 K) [7] without any extensive measures to control the local environment such as optical cavities, plasmonic structures or electrical gating. These favourable properties have enabled experiments with isolated DBT molecules demonstrating fs-timescale spectroscopy [8], photon indistinguishability measurements [9], and environmental acoustic strain characterization [10], while recent theoretical work has investigated the vibrational [11], triplet, and doubly excited states of DBT [12]. A promising environment to house DBT molecules is thin nano-crystals of anthracene [13–17] where the molecules cause little distortion [7] to the van der Waals bonded crystal.

With all solid state emitters it is essential that the temperature dependence and nature of the phonon coupling and decoherence effects are well characterised and understood [18]. These affect the efficiency and indistinguishability of a solid-state single photon source and must be carefully taken into account when designing photonic cavity structures or filtering systems which aim to maximise source figures of merit [19, 20]. In this work we present a detailed experimental interrogation of the optical properties of a DBT–anthracene system, and develop a theoretical model which fully captures all observed features, allowing us to uncover the underlying phonon coupling mechanisms. The temperature-dependent spectra shown in Fig. 1(a) have a rich structure, with a ZPL, several additional narrow lines, and broad sidebands. We are able to associate these with, respectively, direct photon emission, photon emission accompanied by one excitation of a localised vibrational mode of the molecule, and simultaneous emission of a photon and a phonon into the anthracene crystal. Closer analysis reveals temperature dependent homogeneous broadening of the ZPL, which in our model arises from anharmonicity captured by second order electron-phonon coupling terms in our Hamiltonian. These findings have implications for efforts in coupling molecules to photonic structures, where the collection efficiency, purity, and indistinguishability of DBT emission is significantly modified by phonon effects [21–25]. Moreover, the DBT-anthracene crystal is an exemplary open quantum system in its own right, and could be used to test fundamental non-equilibrium concepts such as non-Markovianity [26].

Our single molecule spectroscopy experiments [27, 28] were based on a DBT-doped nano-crystal of anthracene, grown using a re-precipitation technique [16]. This was placed in a closed-cycle cryostat incorporated in a confocal microscope shown schematically in Fig. 1(b). A continuous wave laser was used to excite the DBT molecule to a higher vibrational level of the excited state $S_{1,n>0}$. The molecule then rapidly relaxes (in ps) to the purely electronic excited state $S_{1,0}$ before decaying to the ground state manifold $S_{0,n}$. The emitted fluorescence was collected by the confocal microscope and dispersed by a grating onto a CCD camera to measure the spectrum. The excitation laser was also tuned over the $S_{0,0} \leftrightarrow S_{1,0}$ ZPL transition for varying illumination intensity while detecting red-shifted photons from the decay of $S_{1,0} \rightarrow S_{0,n>0}$ to measure a fluorescence excitation spectrum. By splitting this fluorescence on a beamsplitter and monitoring detection times on the two outputs, we measured the second-order intensity correlation function, allowing us to confirm we were dealing with a single DBT molecule. These measurements were then repeated for temperatures from 4.7 K to 40 K. More details

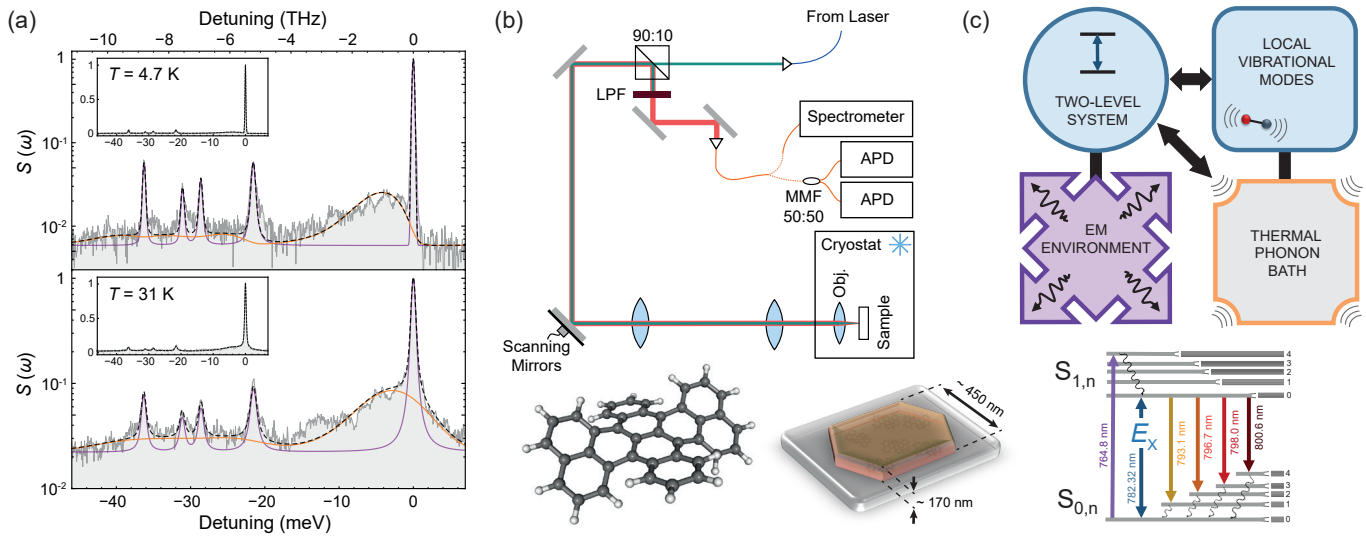

FIG. 1. (a) Single DBT molecule emission spectra taken at 4.7 K (top) and 31 K (bottom). Black-dashed lines show the full theoretical model and grey-solid lines show experimental data. The theoretical spectrum showing only the zero-phonon-line and local vibrational mode peaks is shown in purple [c.f. Eq. 3], while the broad phonon sideband contribution is shown in orange [Eq. 4]. The insets show the spectra on a linear scale. (b) Simplified schematic of the confocal microscope. Dark green is the pump light, and red is the fluorescence. 90:10: 90% reflection, 10% transmission beam-splitter; Obj.: Objective lens; LPF: long-pass filter; MMF 50:50: 50% reflection, 50% transmission multimode fiber beam splitter; APD: avalanche photodiode. The nano-crystal sample (bottom right) consists of DBT (bottom left) embedded in anthracene. (c) Open quantum system model of a single DBT molecule. The system (blue) contains a two level electronic system (TLS) coupled to a discrete set of vibrational modes and an electromagnetic environment. The thermal phonon bath originates from the nano-crystal and is coupled separately to both system elements. The arrows connected to the TLS represent a non-Markovian interaction including feedback. The schematic energy level diagram shows the ground S_0 and excited S_1 electronic singlet states with energy splitting $E_{\rm X}$, and local vibrational modes, all broadened by the thermal phonon environment.

can be found in the Supplementary Information [29].

Inspired by the spectra in Fig. 1(a) our model of a DBT doped anthracene nano-crystal is shown schematically in Fig. 1(c). It consists of a two-level-system (TLS) with ground and excited states $|g\rangle$ and $|e\rangle$ split by energy $E_{\rm X}$, coupled to the electromagnetic (EM) field, harmonic oscillators representing localised vibrational modes of the molecule, and a thermal phonon bath of the anthracene crystal. We treat the TLS and localised vibrational modes within our system degrees of freedom, and thus capture their interactions to all orders. The Hamiltonian of the complete system is

$$H = H_{\rm S} + H_{\rm E} + H_{\rm I}^{\rm EM-TLS} + H_{\rm I}^{\rm PH-TLS} + H_{\rm I}^{\rm PH-LV}, \quad (1)$$

where $H_{\rm S} = E_{\rm X}\sigma^\dagger\sigma + \hbar\sum_{i=1}^{N}[\Delta_i a_i^\dagger a_i + \eta_i\sigma^\dagger\sigma(a_i^\dagger + a_i)]$, with $\sigma = |g\rangle\langle e|$. The N localised modes described by annihilation (creation) operators a_i ($a_i^\dagger$) and energy splittings Δ_i are coupled to the TLS with strengths η_i. The term $H_{\rm E} = \hbar\sum_l \nu_l c_l^\dagger c_l + \hbar\sum_{\mathbf{k}}\omega_{\mathbf{k}} b_{\mathbf{k}}^\dagger b_{\mathbf{k}} + \hbar\sum_{\mathbf{q}} z_{\mathbf{q}} d_{\mathbf{q}}^\dagger d_{\mathbf{q}}$, contains contributions from harmonic baths describing the EM environment with frequencies ν_l and annihilation operators c_l for mode l, and two thermal phonon baths which separately couple to the TLS and local vibrational modes, with frequencies $\omega_{\mathbf{k}}$ and $z_{\mathbf{q}}$ and annihilation operators $b_{\mathbf{k}}$ and $d_{\mathbf{q}}$ for wavevectors $\mathbf{k}$ and $\mathbf{q}$.

The EM environment–TLS interaction term $H_{\rm I}^{\rm EM-TLS}$ gives rise to spontaneous emission, while $H_{\rm I}^{\rm PH-TLS} = H_{\rm I,1}^{\rm PH} + H_{\rm I,2}^{\rm PH}$ couples the phonon bath to the TLS, including terms linear, $H_{\rm I,1}^{\rm PH} = \hbar\sigma^\dagger\sigma\sum_{\mathbf{k}} g_{\mathbf{k}}(b_{\mathbf{k}}^\dagger + b_{\mathbf{k}})$, and quadratic $H_{\rm I,2}^{\rm PH} = \hbar\sigma^\dagger\sigma\sum_{\mathbf{k}\mathbf{k}'} f_{\mathbf{k}\mathbf{k}'}(b_{\mathbf{k}}^\dagger + b_{\mathbf{k}})(b_{\mathbf{k}'}^\dagger + b_{\mathbf{k}'})$ in the phonon displacements, with coupling constants $g_{\mathbf{k}}$ and $f_{\mathbf{k}\mathbf{k}'}$ respectively [30–32]. The linear electron–phonon interaction describes a displacement of the phonon potential well minima. The quadratic term is present as we take the electron–phonon coupling to second-order in the atomic displacements of the crystal lattice, and gives rise to anharmicity of the phonon modes mediated via the TLS [33, 34]. As we will see, the quadratic interaction is crucial for capturing the temperature dependent homogeneous broadening of the ZPL in the emission spectra [35]. The final interaction term $H_{\rm I}^{\rm PH-LV}$ couples the thermal phonon bath to the localized vibrational modes [29].

We now develop a master equation using an extension to the polaron transform approach [19, 36–38], here performing two transformations which displace both the thermal phonon bath and local vibrational modes. The first transformation displaces bath phonons dependent on the TLS state, $b_{\mathbf{k}} \to b_{\mathbf{k}} + \sigma^\dagger\sigma g_{\mathbf{k}}/\omega_{\mathbf{k}}$. This removes the linear TLS–phonon coupling term by moving into a basis which includes the distortion of the anthracene lattice in response to the electronic excitation. This dresses the TLS with phonon degrees of freedom, which when viewed in the original frame, accounts for non-Markovianity between the TLS and the thermal phonon bath. The second transformation acts on the TLS and the localised modes,

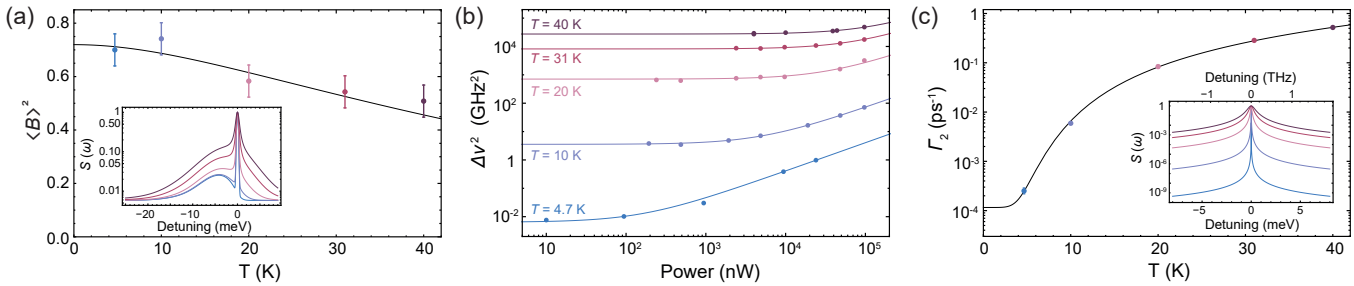

FIG. 2. (a) Debye–Waller factor, $\langle B\rangle^2$, for varying temperature. The solid line shows the theory. The inset shows the calculated spectrum of the ZPL and sideband at temperatures where the data was taken. (b) Squared-linewidths extracted from fluorescence excitation spectra for varying power at different temperatures. Lines are fits to $\Delta\nu^2 = (\Gamma_2/\pi)^2(1+S)$. (c) Experimental values of Γ_2 found from the fits in (b), plotted together with prediction from the theoretical model (solid line). The inset shows the calculated Lorentzian ZPL for temperatures at which the data was taken.

which similarly removes the (linear) interaction terms, and dresses the TLS degrees of freedom with those of the vibrational modes. We then derive a Born-Markov master equation in the polaron frame [19, 36, 37, 39]. In a rotating frame and in the Schrödinger picture, the master equation describing polaron-frame reduced density operator of the TLS and the localised modes is [29]

$$\partial_t\rho(t) = \Gamma_1\mathcal{L}_{\sigma_a}[\rho(t)] + 2\Gamma_2^*(T)\mathcal{L}_{\sigma^\dagger\sigma}[\rho(t)] + \sum_i\Big(-i\Delta_i[a_i^\dagger a_i,\rho(t)] + \Gamma_{i,+}\mathcal{L}_{a^\dagger}[\rho(t)] + \Gamma_{i,-}\mathcal{L}_a[\rho(t)]\Big), \quad (2)$$

where $\mathcal{L}_A[\rho(t)] = A\rho(t)A^\dagger - \frac{1}{2}\{A^\dagger A,\rho(t)\}$, $\Gamma_{i,+} = \kappa_i n(\Delta_i)$ and $\Gamma_{i,-} = \kappa_i(n(\Delta_i)+1)$ with $n(\Delta) = (e^{\hbar\Delta/k_BT}-1)^{-1}$. The first term in Eq. (2) originates from the TLS-EM field interaction and describes spontaneous emission with rate $\Gamma_1 = 1/T_1$ where T_1 is the excited state lifetime. We note that it contains the dressed dipole operator $\sigma_a = \sigma\prod_i\mathcal{B}_i$ with $\mathcal{B}_i = \exp[\eta_i(a_i^\dagger - a_i)/\Delta_i]$, and as such accounts for simultaneous emission of a photon and excitation of localised modes. The second term describes TLS pure-dephasing with temperature dependent rate $\Gamma_2^*(T) \propto \sum_{\mathbf{k},\mathbf{k}'}|f_{\mathbf{k},\mathbf{k}'}|^2 n(\nu_k,T)(n(\nu_k,T)+1)$, derived from the quadratic TLS–phonon bath coupling term. The local vibrational mode absorption and decay rates $\Gamma_{i,\pm}$ depend on κ, which is proportional to the vibrational mode–phonon bath spectral density $J_{\mathrm{PH-LV}}(\omega) = \sum_q|p_q|^2\delta(\omega_q-\omega)$, where p_q are the local vibrational–phonon bath coupling constants. We take a super-Ohmic spectral density $J_{\mathrm{PH-LV}}(\Delta_i) \propto \Delta_i^3/\zeta^2 e^{-\Delta_i/\zeta}$, to reflect the three-dimensional and weak nature of the coupling, where ζ is the phonon bath cut-off frequency [40–42].

The emission spectrum is given by $S(\omega) = \mathrm{Re}[\int_0^\infty d\tau g^{(1)}(\tau)e^{-i\omega\tau}]$ where $g^{(1)}(\tau) = \int_0^\infty dt\,\langle E(t+\tau)^\dagger E(t)\rangle$ is the first order correlation function with $E(t)$ the positive frequency component of the electric field operator. Following Refs. [19, 43], we solve the Heisenberg equations of motion in the polaron frame to find $E(t) = E_0(t) + \sqrt{\Gamma_1/2\pi}\sigma_a(t)B_-(t)$, where $E_0(t)$ is the free field, assumed to be in the vacuum. We note the second source term contains both TLS and thermal phonon bath degrees of freedom, seen through the appearances of σ_a and the phonon bath displacement operator $B_\pm = \exp[\pm\sum_{\mathbf{k}} g_{\mathbf{k}}(b_{\mathbf{k}}^\dagger - b_{\mathbf{k}})/\omega_{\mathbf{k}}]$. We can make use of the varying time scales of the phonon relaxation (~ 1 ps) and photon emission (~ 1 ns) to factorise the correlation function, finding $g^{(1)}(\tau) \approx (\Gamma_1/2\pi)g_0^{(1)}(\tau)\mathcal{G}(\tau)$ where $\mathcal{G}(\tau) = \langle B\rangle^2\exp[\phi(\tau)]$, with $\phi(\tau) = \int_0^\infty d\omega J_{\mathrm{PH}}(\omega)\omega^{-2}(\coth(\hbar\beta\omega/2)\cos(\omega\tau) - i\sin(\omega\tau))$ and $\langle B\rangle = \exp[-\phi(0)/2]$ [19, 44]. The electron–phonon spectral density introduced here is $J_{\mathrm{PH}}(\omega) = \sum_{\mathbf{k}} g_{\mathbf{k}}^2\delta(\omega-\omega_{\mathbf{k}})$, while $g_0^{(1)}(\tau) = \int_0^\infty dt\,\langle\sigma_a^\dagger(t+\tau)\sigma_a(t)\rangle$. We find the emission spectrum can therefore be written $S(\omega) \propto S_{\mathrm{ZPL+LV}}(\omega) + S_{\mathrm{SB}}(\omega)$, where

$$S_{\mathrm{ZPL+LV}}(\omega) = \langle B\rangle^2\,\mathrm{Re}\Big[\int_0^\infty d\tau g_0^{(1)}(\tau)e^{-i\omega\tau}\Big], \quad (3)$$

describes peaks associated with the ZPL and localised phonon modes, and

$$S_{\mathrm{SB}}(\omega) = \mathrm{Re}\Big[\int_0^\infty d\tau g_0^{(1)}(\tau)(\mathcal{G}(\tau) - \langle B\rangle^2)e^{-i\omega\tau}\Big]. \quad (4)$$

describes a broad phonon sideband complementing each peak. A key advantage of working in the polaron frame is that the correlation function $g_0^{(1)}(\tau)$ can be found using the (Markovian) quantum regression theorem [45, 46], while non-Markovian interactions necessary to capture phonon sidebands are naturally captured by the phonon bath correlation function $\mathcal{G}(\tau)$ in Eq. (4). Furthermore, by writing the spectrum in this way we can immediately see that the Debye–Waller factor (fraction of light not emitted into sidebands) is given by $\int S_{\mathrm{ZPL+LV}}(\omega)d\omega/\int S(\omega)d\omega = \langle B\rangle^2$.

Predictions of our model are shown by the black dashed curves in Fig. 1(a). The peak at zero detuning corresponds to the ZPL at 782.32 nm, while the other prominent peaks arise from local vibrations of the DBT molecule excited during the photon emission process [33, 47]. We find $N = 4$ separate DBT vibrational modes are needed to reproduce these features. The fitted mode energies $\hbar\Delta_i$ are consistent (to within 2%) with previous works [11], and are listed in the Supplementary Information together with the fitted coupling constants

η_i. To achieve good fits we found it necessary to include only the ground and first excited state for each mode in our calculations, meaning that higher vibronic transitions contribute little to the observed spectra.

The purple curves in Fig. 1(a) show the calculated spectra including only the ZPL and local vibrational mode peaks using Eq. (3), while the orange curves show the phonon sideband contribution given in Eq. (4). The shape of the sideband depends on the functional form of the spectral density $J_{\mathrm{PH}}(\omega)$ which characterises the frequency spectrum of the electron–phonon coupling. We use the super Ohmic form $J_{\mathrm{PH}}(\omega) = \alpha\,\omega^3 \exp\left[-\omega^2/\xi^2\right]$, where α captures the overall TLS–phonon bath coupling strength, and $\xi = \sqrt{2}v/d$ is a high-frequency cut-off to reflect the suppression of coupling to phonons whose wavelengths are much smaller than the size of the DBT molecule d, where v is the speed of sound in anthracene. These parameters are extracted from fits to the emission spectra. This form is similar to that used to capture excitation-induced dephasing and phonon sidebands in semiconductor QDs, and can be derived by approximating the electronic ground and excited states as Gaussian wavefunctions [19, 36, 37, 43, 48, 49].

The fraction of the emission which goes into the ZPL and local vibrational mode peaks is given by the Debye–Waller factor, which in our theory is equal to the square of the average phonon bath displacement $\langle B\rangle^2 = \exp[-\int_0^\infty J_{\mathrm{PH}}(\omega)\omega^{-2}\coth(\beta\omega/2)d\omega]$. This is plotted as a function of temperature in Fig. 2(a), together with the corresponding experimentally extracted values. We see that for this molecule we have a maximum ZPL fraction of 72%. This is lower than expected for DBT and could partially account for the reduction in coupling observed recently for single molecules in open-access microcavities compared to their predictions [21, 25]. However, the observed fraction could also be due to the close proximity of surfaces in the nano-crystal host used in these experiments [50], and further tests with co-sublimation grown crystals [14] may yield a different result.

Broadening of the emission lines in the spectra is captured by the dissipators in Eq. (2). Of particular interest is the homogeneous broadening of the ZPL with temperature. In our model this broadening follows $\Gamma_2(T) = \Gamma_1/2 + \Gamma_2^*(T)$, where $\Gamma_2^*(T)$ is a phonon-induced pure dephasing rate. To investigate this broadening in a way that is not affected by the resolution of the spectrometer, we compare our model to measured fluorescence excitation spectra of the ZPL for varying excitation power, measured outside the cryostat before the objective lens. The results at various temperatures are shown in Fig. 2(b). The width of the measured Lorentzian lines can be expressed as $\Delta\nu = \Gamma_2/\pi\sqrt{1+S}$ with saturation parameter S, allowing us to find Γ_2 by extrapolating the width to zero power [47]. The extracted $\Gamma_2(T)$ are shown in Fig. 2(c), together with the theoretical prediction. This molecule was slightly broadened at our lowest achievable temperature of 4.7 K, and our model predicts cooling below 3 K would be sufficient to reach a lifetime-limited linewidth ($\Gamma_2 = \Gamma_1/2$). The broadening originates from mixing between vibronic states induced by anharmonic effects. This requires the participation of two phonons from the residual bath, and as such necessitates the inclusion of quadratic terms in our Hamiltonian to be captured. Furthermore, the phonon absorption process results in a strong temperature dependence which our model accurately predicts.

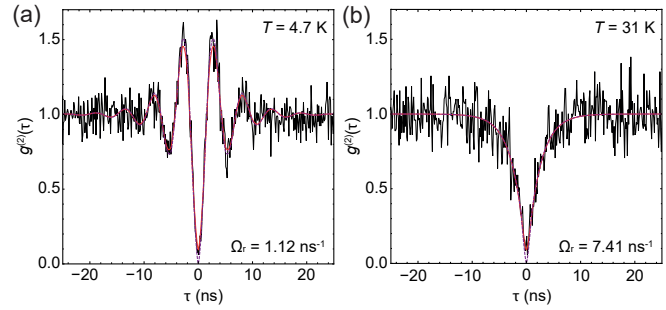

FIG. 3. Measured $g^{(2)}(\tau)$ taken from the DBT molecule at (a) 4.7 K and (b) 31 K. Black shows the experimental data. Red solid lines show the theoretical model convolved with a Gaussian function to account for the detector timing jitter and purple dashed lines show the model without convolution.

To further demonstrate the versatility of our model, we now investigate the time-domain dynamics of the DBT molecule by measuring the second-order intensity correlation function under continuously driven resonant excitation conditions [51]. To do so we introduce an additional driving term $H_{\mathrm{DR}} = \frac{\Omega}{2}(\sigma + \sigma^\dagger)$ to the system Hamiltonian H_{S} defined in Eq. (1), with Rabi frequency Ω. This results in a slightly modified master equation [29]. The normalised intensity correlation function is then $g^{(2)}(\tau) = \left\langle E^\dagger E^\dagger(\tau)E(\tau)E\right\rangle_{\mathrm{ss}} / \left\langle E^\dagger E\right\rangle_{\mathrm{ss}}^2$, where averages are calculated in the steady-state, and τ is the time delay between detection events [47]. The calculated $g^{(2)}(\tau)$ and experimental data are shown in Fig. 3, for temperatures of 4.7 K in (a) and 31 K in (b). This measurement probes the excited state population of the molecule conditioned on being in the ground state at $\tau = 0$. The dip at $\tau = 0$ reflects the strong suppression of multi-photon emission events and is characteristic of a single photon source. At $T = 4.7$ K Rabi oscillations can be seen, which represent the coherent exchange of excitations from the driving laser to the system. For our calculations we take the molecular parameters extracted from the experimentally measured spectra, with the Rabi frequency Ω as the only additional fitting parameter. Interestingly, the bare Rabi frequency Ω that gives the best fit is not the observed Rabi frequency of the oscillations in Fig. 3(a). Instead a value of $\Omega_r = \Omega\,\langle B\rangle \prod_i \langle \mathcal{B}_i\rangle$ is observed, which accounts for renormalisation of the bare Rabi frequency arising from phonon coupling [52]. At higher temperatures phonon interactions increasingly damp these oscillations, as is the case in Fig. 3(b).

We have presented a joint experiment–theory analysis that comprehensively describes the emission proper-

ties of a single DBT molecule encased in an anthracene nano-crystal. The model captures the zero-phonon-line, four peaks associated with local vibrational modes of the molecule, phonon sidebands, and a temperature dependent homogeneous broadening of the ZPL which arises when we include anharmonic effects by taking the electron–phonon interaction to second order. These findings have important consequences for the use of molecules as single photon sources in quantum information applications [53]. The photon indistinguishability is the square of the probability of emission into the ZPL multiplied by its coherence, and our model gives $\mathcal{I} = [\prod_i \langle \mathcal{B}_i \rangle^4] \langle B \rangle^4 \Gamma_1/(2\Gamma_2)$, which we see is strongly affected by the various phonon related features that we identify. Our work constitutes a natural starting point for future studies investigating effects associated with the coupling of molecules to optical waveguides [22–24] and cavities [21, 25, 54]. The model could be extended in the future to other promising solid-state quantum emitters for which phonon coupling effects are important, such as defects in crystals and two-dimensional materials.

We thank Jon Dyne and Dave Pitman for their expert mechanical workshop support. This work was supported by EPSRC (EP/P030130/1, EP/P01058X/1, EP/R044031/1, EP/S023607/1, and EP/L015544/1), the Royal Society (UF160475), and the EraNET Cofund Initiative QuantERA under the European Union's Horizon 2020 research and innovation programme, Grant No. 731473 (ORQUID Project). J.I.-S. acknowledges support from the Royal Commission for the Exhibition of 1851.

Near the completion of this work we became aware of a similar theoretical study investigating the optics of molecular systems encased in crystals [55].

[1] M. D. Eisaman, J. Fan, A. Migdall, and S. V. Polyakov, Rev. Sci. Instrum. **82** (2011).
[2] E. Knill, R. Laflamme, and G. Milburn, Nature **409**, 49 (2000).
[3] W. E. Moerner, New J. Phys. **6**, 88 (2004).
[4] P. Siyushev, G. Stein, J. Wrachtrup, and I. Gerhardt, Nature **509**, 66 (2014).
[5] J.-B. Trebbia, H. Ruf, P. Tamarat, and B. Lounis, Opt. Express **17**, 23986 (2009).
[6] K. G. Schädler, C. Ciancico, S. Pazzagli, P. Lombardi, A. Bachtold, C. Toninelli, A. Reserbat-Plantey, and F. H. L. Koppens, Nano Lett. **19**, 3789 (2019).
[7] A. A. L. Nicolet, P. Bordat, C. Hofmann, M. A. Kol'chenko, B. Kozankiewicz, R. Brown, and M. Orrit, ChemPhysChem **8**, 1929 (2007).
[8] M. Liebel, C. Toninelli, and N. F. Van Hulst, Nature Photonics **12**, 45 (2018).
[9] J. B. Trebbia, P. Tamarat, and B. Lounis, Physical Review A - Atomic, Molecular, and Optical Physics **82**, 1 (2010).
[10] Y. Tian, P. Navarro, and M. Orrit, Phys. Rev. Lett. **113**, 135505 (2014).
[11] I. Deperasiǹska, E. Karpiuk, M. Banasiewicz, A. Makarewicz, and B. Kozankiewicz, Phys. Chem. Chem. Phys. **13**, 1872 (2011).
[12] Z. S. Sadeq, R. A. Muniz, and J. E. Sipe, Phys. Rev. Materials **2**, 075202 (2018).
[13] A. A. L. Nicolet, P. Bordat, C. Hofmann, M. A. Kol'chenko, B. Kozankiewicz, R. Brown, and M. Orrit, ChemPhysChem **8**, 1215 (2007).
[14] K. D. Major, Y.-H. Lien, C. Polisseni, S. Grandi, K. W. Kho, A. S. Clark, J. Hwang, and E. A. Hinds, Rev. Sci. Instrum. **86**, 083106 (2015).
[15] C. Polisseni, K. D. Major, S. Boissier, S. Grandi, A. S. Clark, and E. A. Hinds, Opt. Express **24**, 5615 (2016).
[16] S. Pazzagli, P. Lombardi, D. Martella, M. Colautti, B. Tiribilli, F. S. Cataliotti, and C. Toninelli, ACS Nano **12**, 4295 (2018).
[17] R. Schofield, K. D. Major, S. Grandi, S. Boissier, E. Hinds, and A. S. Clark, J. Phys. Commun. **2**, 115027 (2018).
[18] J. Friedrich and D. Haarer, Angew. Chem. Int. Ed. Engl. **23**, 113 (1984).
[19] J. Iles-Smith, D. P. S. McCutcheon, A. Nazir, and J. Mørk, Nat. Photon. **11**, 521 (2017).
[20] P. Lodahl, S. Mahmoodian, and S. Stobbe, Rev. Mod. Phys. **87**, 347 (2015).
[21] D. Wang, H. Kelkar, D. Martin-Cano, T. Utikal, S. Götzinger, and V. Sandoghdar, Phys. Rev. X **7**, 021014 (2017).
[22] P. Türschmann, N. Rotenberg, J. Renger, I. Harder, O. Lohse, T. Utikal, S. Götzinger, and V. Sandoghdar, Nano Lett. **17**, 4941 (2017).
[23] P. Lombardi, A. P. Ovvyan, S. iPazzagli, G. Mazzamuto, G. Kewes, O. Neitzke, N. Gruhler, O. Benson, W. H. P. Pernice, F. S. Cataliotti, and C. Toninelli, ACS Photonics **5**, 126 (2018).
[24] S. Grandi, M. P. Nielsen, J. Cambiasso, S. Boissier, K. D. Major, C. Reardon, T. F. Krauss, R. F. Oulton, E. A. Hinds, and A. S. Clark, APL Photonics **4**, 086101 (2019).
[25] D. Wang, H. Kelkar, D. Martin-Cano, D. Rattenbacher, A. Shkarin, T. Utikal, S. Götzinger, and V. Sandoghdar, Nat. Phys. **15**, 483 (2019).
[26] I. de Vega and D. Alonso, Rev. Mod. Phys. **89**, 015001 (2017).
[27] T. Plakhotnik, E. A. Donley, and U. P. Wild, Annu. Rev. Phys. Chem. **48**, 181 (1997).
[28] P. Tamarat, A. Maali, B. Lounis, and M. Orrit, J. Phys. Chem. A **104**, 1 (2000), https://doi.org/10.1021/jp992505l.
[29] See the Supplementary Information for more details of the experimental methods and the theoretical model, and which includes Refs. [56–58].
[30] F. Giustino, Rev. Mod. Phys. **89**, 015003 (2017).
[31] L. M. Woods and G. D. Mahan, Phys. Rev. B **57**, 7679 (1998).
[32] G. Mahan, *Many-Particle Physics*, Physics of Solids and Liquids (Springer US, 2013).
[33] P. de Bree and D. A. Wiersma, J. Chem. Phys. **70**, 790 (1979).
[34] P. Machnikowski, Phys. Rev. Lett. **96**, 140405 (2006).
[35] E. A. Muljarov and R. Zimmermann, Phys. Rev. Lett. **93**, 237401 (2004).
[36] A. Nazir and D. P. S. McCutcheon, J. Phys. Condens. Matter **28** (2016).
[37] D. P. S. McCutcheon and A. Nazir, New J. Phys. **12**, 113042 (2010).
[38] K. Roy-Choudhury and S. Hughes, Phys. Rev. B **92**, 205406 (2015).
[39] H. P. Breuer and F. Petruccione, *The theory of open*

quantum systems (Oxford University Press, 2002).
[40] A. O. Caldeira and A. J. Leggett, Phys. Rev. Lett. **46**, 211 (1981).
[41] F. Gottwald, S. Ivanov, and O. Khn, The Journal of Chemical Physics **144** (2016), 10.1063/1.4946872.
[42] J. Paavola, J. Piilo, K.-A. Suominen, and S. Maniscalco, Phys. Rev. A **79**, 052120 (2009).
[43] J. Iles-Smith, D. P. S. McCutcheon, J. Mørk, and A. Nazir, Phys. Rev. B **95**, 201305 (2017).
[44] C. Roy and S. John, Phys. Rev. A **81**, 023817 (2010).
[45] D. P. S. McCutcheon, Phys. Rev. A **93**, 022119 (2016).
[46] G. Guarnieri, A. Smirne, and B. Vacchini, Phys. Rev. A **90**, 022110 (2014).
[47] S. Grandi, K. D. Major, C. Polisseni, S. Boissier, A. S. Clark, and E. A. Hinds, Phys. Rev. A **94**, 063839 (2016).
[48] A. Brash, J. Iles-Smith, C. L. Phillips, D. P. S. McCutcheon, J. O'Hara, E. Clarke, B. Royall, J. Mørk, M. S. Skolnick, A. M. Fox, and A. Nazir, Phys. Rev. Lett. **123**, 167403 (2019).
[49] A. Reigue, J. Iles-Smith, F. Lux, L. Monniello, M. Bernard, F. Margaillan, A. Lemaitre, A. Martinez, D. P. S. McCutcheon, J. Mørk, R. Hostein, and V. Voliotis, Phys. Rev. Lett. **118**, 233602 (2017).
[50] B. Gmeiner, A. Maser, T. Utikal, S. Gtzinger, and V. Sandoghdar, Phys. Chem. Chem. Phys. **18**, 19588 (2016).
[51] G. Wrigge, I. Gerhardt, J. Hwang, G. Zumofen, and V. Sandoghdar, Nature Physics **4**, 60 (2008).
[52] D. P. S. McCutcheon and A. Nazir, Phys. Rev. Lett. **110**, 217401 (2013).
[53] M. Rezai, J. Wrachtrup, and I. Gerhardt, Phys. Rev. X **8**, 031026 (2018).
[54] M. Reitz, C. Sommer, and C. Genes, Phys. Rev. Lett. **122**, 203602 (2019).
[55] M. Reitz *et al.*, "Molecule-photon interactions in phononic environments," (2019), arxiv:1912.02635.
[56] S. Scheel, L. Knöll, D.-G. Welsch, and S. M. Barnett, Phys. Rev. A **60**, 1590 (1999).
[57] H. B. Huntington, S. G. Gangoli, and J. L. Mills, J. Chem. Phys. **50**, 3844 (1969).
[58] R. C. Dye and C. J. Eckhardt, J. Chem. Phys. **90**, 2090 (1989).